



Thermal Reactions between H₂S and O₃: Implications for Europa Surface Chemistry

Patrick D. Tribbett¹ and Mark J. Loeffler^{1,2} ¹ Department of Astronomy and Planetary Science, Northern Arizona University, Flagstaff, AZ 86011, USA; pdt43@nau.edu² Center for Materials Interfaces in Research and Applications (MIRA), Northern Arizona University, Flagstaff, AZ 86011, USA

Received 2022 June 27; revised 2022 September 8; accepted 2022 September 13; published 2022 October 18

Abstract

Here we present a laboratory study demonstrating a low-temperature thermal oxidation reaction within H₂O + H₂S + O₃ solid ice mixtures that produces observable sulfur anion products at temperatures as low as 90 K. This reaction primarily produces SO₂, sulfur anions (including HSO₃[−], HSO₄[−], and SO₄^{2−}), and O₂ at lower temperatures (90–140 K) and hydrated states of sulfuric acid (H₂SO₄ · nH₂O, where n = 0, 1, 4) at higher temperatures (150–250 K). We estimate that the overall activation energy to initiate these reactions is 20 ± 3 kJ mol^{−1}, which is significantly lower than the activation energy required to oxidize SO₂ to the sulfate ion. Given the detection of sulfur species on the surfaces of the Galilean satellites and the prevalence of radiolytically produced oxidants, we expect that these thermal reactions will play an important role in explaining the results obtained from future observations and missions that can measure the spatial distribution of these species.

Unified Astronomy Thesaurus concepts: Laboratory astrophysics (2004); Astrochemistry (75); Surface ices (2117); Galilean satellites (627)

1. Introduction

The radiolytic chemistry of icy surfaces within the solar system and in the interstellar medium (ISM) has been studied for several decades. However, the thermal chemistry of surface and subsurface ices has received significantly less attention due to the characteristically low temperatures (~60–160 K on the Galilean and Saturnian satellites (Squyres 1980; Hanel et al. 1982; Spencer et al. 1999); ~20–40 K in the outer solar system (Stern et al. 1993; Earle et al. 2017); ~10 K in the ISM; Caselli & Ceccarelli 2012). Despite the low temperatures in these astronomical environments and the limited diffusion associated with solid-state materials, recent studies have demonstrated that many chemical systems are thermally reactive at temperatures as cold as 80 K (Moore et al. 2007; Bossa et al. 2008; Loeffler & Hudson 2010). Low-temperature acid–base reactions (Demyk et al. 1998; Noble et al. 2013) proceed through proton transfer, and increasingly complex reaction mechanisms, including oxidation reduction (Loeffler & Hudson 2013, 2016) and nucleophilic additions (Bossa et al. 2008; Noble et al. 2012), also occur at low temperatures. For a recent review of thermally reactive astrochemical systems, see Theulé et al. (2013).

One environment of particular interest is the Galilean system, which is exposed to substantial ionizing radiation (Cooper et al. 2001; Nordheim et al. 2019), is geologically active (Greeley et al. 2004), and possesses surface and near-surface diurnal temperatures potentially conducive to low-temperature thermal reactions (Spencer et al. 1999). Decades of laboratory studies have demonstrated that the irradiation (H⁺ and e[−]) of H₂O ice produces a number of radiolytic products, including H₂, O₂, and H₂O₂ (Moore & Hudson 2000; Orlando & Sieger 2003; Loeffler et al. 2006a; Zheng et al. 2006). If enough radiolytic O₂ is produced, O₃ will also be produced, as has been shown directly in experiments that deposited H₂O ice, while actively irradiating the sample with heavy ions

(Teolis et al. 2006). Despite the overwhelming number of laboratory studies demonstrating solid-state radiolysis and the production of strong oxidants (H₂O₂ and O₃) and a magnetospheric radiation environment encompassing the Galilean satellites, the observational evidence for these two solid-state species is both underwhelming and complex. In fact, only H₂O₂ has been definitively observed on Europa’s surface, and it is largely confined to the leading hemisphere (Carlson et al. 1999b; Hand & Brown 2013). Conversely, O₃ has only been detected in ultraviolet reflectance spectra of the trailing hemisphere of Ganymede (Noll et al. 1996). While it seems likely that the conditions of the local surface environment (radiation flux, composition, temperature, etc.) strongly influence the formation and survival of these two species, to date, there is no unanimously accepted solution that can explain these observations.

Interestingly, Noll et al. (1997) noted a possible anticorrelation between these oxidant populations and other resident species, specifically sulfur species. SO₂ is largely confined to the trailing hemisphere of Europa (Hendrix et al. 2011), while H₂O₂ has primarily been detected on the leading hemisphere (Hand & Brown 2013). Low-temperature thermal reactions may play an important role in these hemispheric dichotomies, especially in the near subsurface. Previous laboratory studies by Loeffler & Hudson (2013, 2016) demonstrate that SO₂ reacts readily with both H₂O₂ and O₃ at temperatures as low as 80 K. For a recent review of sulfur ice astrochemistry, see Mifsud et al. (2021a). In addition, H₂S has been tentatively identified on the surface of the Galilean satellites (McCord et al. 1998). Though H₂S does not react with the oxidant H₂O₂ in the solid phase (Loeffler & Hudson 2015), H₂S reacts readily with the oxidant O₃ in the gas phase (Cadle & Ledford 1966; Hales et al. 1969; Glavas & Toby 1975). A low-temperature thermal oxidation reaction between an additional sulfur compound and the strong oxidant O₃ may have implications for the surface and subsurface chemistry of the Galilean satellites. Here we demonstrate the efficacy of a thermal oxidation reaction within H₂O + H₂S + O₃ ice mixtures at temperatures relevant to the icy satellites. We identify the



Original content from this work may be used under the terms of the [Creative Commons Attribution 4.0 licence](https://creativecommons.org/licenses/by/4.0/). Any further distribution of this work must maintain attribution to the author(s) and the title of the work, journal citation and DOI.

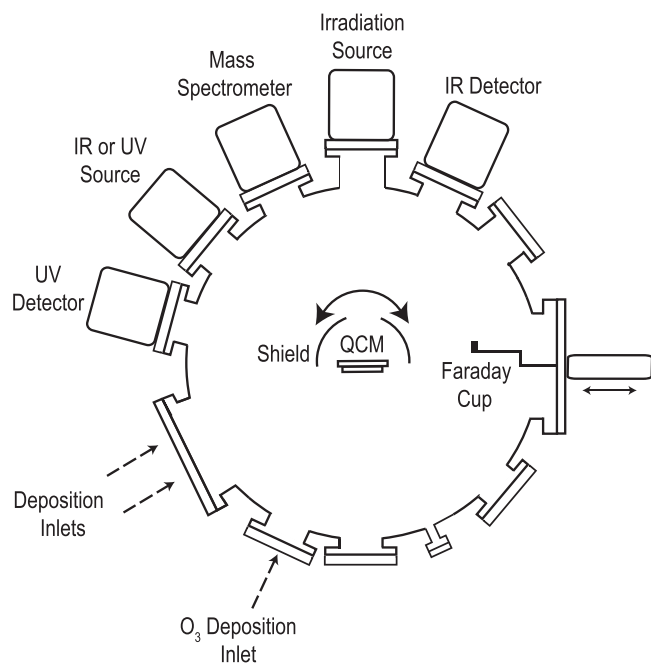


Figure 1. Experimental setup.

reaction products using a combination of infrared (IR) spectroscopy, microbalance gravimetry, and mass spectrometry (MS) as our analytical tools. In addition, we derive an overall reaction activation energy and discuss this reaction's implications for Europa, Ganymede, and Callisto in anticipation of the upcoming NASA Europa Clipper Mission.

2. Experimental Methods

We performed all experiments within a stainless steel ultrahigh-vacuum (UHV) chamber with a base pressure of 10^{-9} torr ($\sim 10^{-10}$ torr within the thermal radiation shield). Figure 1 shows the current setup used for this study, which has been slightly modified from our recent work (Tribbett et al. 2021; Tribbett & Loeffler 2021). To prepare our samples, we codeposited H_2O (high-performance liquid chromatography grade, Sigma Aldrich), H_2S (99.95% purity, Matheson Gas), and O_3 at 50 K from separate mixing lines onto an optically flat gold mirror electrode of an Inficon IC6 quartz crystal microbalance (QCM). We produced O_3 within a glass manifold filled with O_2 (99.999% purity, Matheson Gas) by sparking the manifold with a Tesla coil for ~ 20 minutes. The resultant O_3 condensed in a portion of the manifold submerged in a liquid nitrogen bath, and all residual O_2 was pumped away. We determined the composition of our $\text{H}_2\text{O} + \text{H}_2\text{S} + \text{O}_3$ ($71:23:6 \pm 2:2:1$) ices by first leaking in a small amount of H_2O , then adding H_2S , and finally adding in O_3 , all while monitoring the change in deposition rate with our QCM. The amount of pure H_2O and $\text{H}_2\text{O} + \text{H}_2\text{S}$ was $\sim 5\%$ of the total mass of the sample, and the derived composition includes these first two layers. We estimate that the uncertainty of our composition measurements due to the unmixed layers is less than 5%, which is within the reproducibility of our growth conditions. We estimate the thickness of our mixture to be $\sim 0.85\text{--}1\text{ }\mu\text{m}$, assuming a density of 0.82 g cm^{-3} for H_2O (Westley et al. 1998), 1.65 g cm^{-3} for O_3 (Teolis et al. 2007a; Raut et al. 2011), and 1.15 g cm^{-3} for H_2S . Due to the sparse density measurements of solid H_2S and the density's

dependence on deposition method (Loeffler et al. 2016), we opted to determine the density of amorphous H_2S deposited at 50 K within our UHV chamber using ultraviolet-visible spectroscopy (see Behr et al. 2020 for additional information regarding the methods). Our derived density of 1.15 g cm^{-3} is consistent with the Lorentz–Lorenz estimate by Hudson & Gerakines (2018; $\sim 1.1\text{ g cm}^{-3}$) for background deposited amorphous H_2S ice and the more recent measurement by Yarnall & Hudson (2022a) for crystalline H_2S ice (1.22 g cm^{-3}).

We monitored the ice samples using a combination of IR spectroscopy, MS, and the QCM. We acquired specular reflectance spectra between $10,000$ and 650 cm^{-1} using the IR light source from a Thermo-Nicolet iS50 Fourier Transform Infrared Spectrometer that is incident on the sample at 37.5° , and analyzed the reflected light using an MCT-A detector at a spectral resolution of 2 cm^{-1} . Here we report spectra in units of optical depth ($-\ln(R/R_0)$), where R is the reflected intensity from the sample, and R_0 is the reflected intensity from the bare gold substrate.

Once the ice samples were deposited, we performed one of two heating approaches: linear heating or isothermal annealing. During the linear heating experiments, we warmed the ice samples from 50 to 290 K at a rate of 0.1 K minute^{-1} while monitoring for reactions using IR spectroscopy and the QCM. The QCM data indicated that sublimation of O_3 within a H_2O -ice matrix between 50 and 130 K is negligible (see Section 3). However, the band area of the O_3 combination band at 2104 cm^{-1} decreases by $\sim 15\%$ between 50 and 130 K, which is consistent with Loeffler & Hudson (2016) and taken into account in our analysis. During the isothermal annealing experiments, we warmed the ice samples from 50 K to an annealing temperature between 95 and 125 K at a rate of 5.0 K minute^{-1} . The samples remained at the annealing temperature for 24 hr, where we monitored them using IR spectroscopy to derive reaction kinetic parameters (Loeffler & Hudson 2013). To determine the extent of the reaction, we monitored the 2104 cm^{-1} O_3 band, since sulfur anion products appear and overlap with the stronger fundamental O_3 feature at 1032 cm^{-1} (Teolis et al. 2007a; Loeffler & Hudson 2016). Lastly, during both warming techniques, we monitored the composition of the ejected flux using a Stanford Research Systems (SRS 100) Residual Gas Analyzer, aimed at an incident angle of $\sim 19^\circ$ with respect to the QCM substrate.

3. Results

Figure 2 shows the mid-IR spectrum of a $\text{H}_2\text{O} + \text{H}_2\text{S} + \text{O}_3$ ice mixture after deposition at 50 K and at several temperatures during warming to 150 K at a rate of 0.1 K minute^{-1} . The initial spectrum is dominated by several large absorption features attributed to H_2O (O–H bending mode, 1654 cm^{-1} ; lattice mode, 806 cm^{-1}) and H_2S (S–H stretching modes, 2551 cm^{-1} ; S–H bending mode, 1175 cm^{-1}), as well as several sharper peaks attributed to O_3 (1032 and 2104 cm^{-1}). Spectral assignments for these reactants can be found in Table 1. We note that there is a small amount of CO_2 and OCS contamination within our ice mixture, indicated with asterisks in the 150 K spectrum. The CO_2 is evident by the absorption feature between 2400 and 2300 cm^{-1} (C = O stretch). Instead of using the band strength of the CO_2 (Gerakines et al. 1995; Gerakines & Hudson 2015), which can be problematic due to the interference effects typical of thin film reflectance

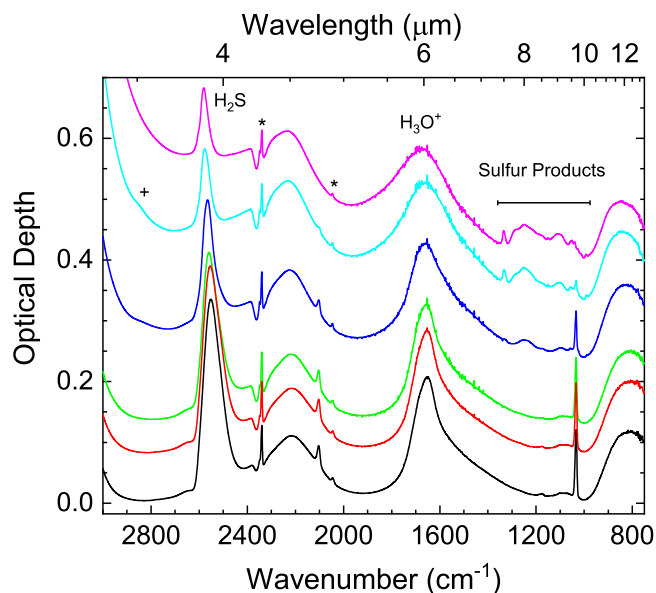


Figure 2. The IR spectra of a $\text{H}_2\text{O} + \text{H}_2\text{S} + \text{O}_3$ sample (75:20:5) during warming at a rate of $0.1 \text{ K minute}^{-1}$. The spectra correspond to approximate temperatures of (bottom to top) 50, 71, 91, 110, 130, and 151 K. Asterisks denote contaminants within the ice (CO_2 and OCS). The plus sign corresponds to the H_2O_2 band at $\sim 2850 \text{ cm}^{-1}$.

spectroscopy (Teolis et al. 2007b), we estimated the CO_2 column density by codepositing a mixture with known amounts of H_2O and CO_2 to a thickness of $\sim 0.85\text{--}1 \mu\text{m}$ and compared the integrated band area of the fundamental CO_2 feature to the integrated band area of the feature in our $\text{H}_2\text{O} + \text{H}_2\text{S} + \text{O}_3$ ice. With this approach, we determined the amount of CO_2 in our ice mixtures to be $\sim 1.10 \times 10^{15} \text{ CO}_2 \text{ cm}^{-2}$, or $\sim 0.04\%$ of our sample by number. Regardless, previous work has shown that CO_2 is not oxidized by O_3 at these temperatures and thus does not participate in the observed reactions (Loeffler & Hudson 2016). CO_2 has also been shown to react with H_2O to create H_2CO_3 , or carbonic acid; however, this reaction is endothermic (31.4 kJ mol^{-1}) and unlikely to occur at low temperatures in the absence of ionizing radiation (Zheng & Kaiser 2007). The OCS contamination is apparent from the small band centered at 2045 cm^{-1} (Ferrante et al. 2008) and is likely introduced by the H_2S source, which lists OCS as a possible contaminant at 0.2% by volume. Despite being fairly dilute, the band strength for the $\text{C}=\text{O}$ stretch of OCS is comparable to CO_2 (Yarnall & Hudson 2022b), and minimal contamination from this compound is reasonable. Moreover, this feature can be seen in the spectra of mixtures of H_2S and H_2O ice throughout the literature, where similar qualities of H_2S are used (Jiménez-Escobar & Caro 2011; Yarnall & Hudson 2022b). Recent work has demonstrated that OCS can undergo thermal nucleophilic addition in the presence of methylamine (CH_3NH_2 ; Mahjoub & Hodyss 2018); however, the kinetics of a simple addition reaction between OCS and H_2O are unfavorable (Ghosh et al. 2010). Given the minimal change in band area and shape during our experiments and the minor amount present, it is also unlikely that OCS contributes to our thermal reactions with O_3 . Regardless, we hope to investigate this as a chemical system ($\text{H}_2\text{O} + \text{OCS} + \text{O}_3$) in the future.

During warming, both H_2S and O_3 absorption features begin to decrease by around 70 K despite negligible mass loss from the sample at these temperatures (Figure 4). We suspect that

this decrease corresponds to the formation of an intermediate sulfur compound that we cannot uniquely identify with IR spectroscopy (see Section 4.1 for more details; Glavas & Toby 1975). Above 90 K, several spectral changes include the broadening of the H_2O bending feature and the appearance of HSO_3^- (1038 cm^{-1}), HSO_4^- (992 cm^{-1}), SO_4^{2-} (1111 cm^{-1}), and the broader feature at 1235 cm^{-1} , which has been attributed to both the bisulfite and bisulfate anions (Moore et al. 2007; Loeffler & Hudson 2016). Above 110 K, an additional band attributed to HSO_3^- appears at 1013 cm^{-1} , and two sharp stretching bands of SO_2 appear at 1333 and 1149 cm^{-1} . Several of these smaller features are more evident in Figure 3, which highlights the wavelength region ($1400\text{--}800 \text{ cm}^{-1}$) most affected by the presence of the sulfur anions. Additionally, we see the appearance (between 110 and 130 K) and disappearance (150 K) of a small band at 2848 cm^{-1} , which we attribute to H_2O_2 (Loeffler et al. 2006a; Zheng et al. 2006). The feature's disappearance at temperatures below where it will sublime (Loeffler et al. 2006b) is consistent with known thermally driven reactions between H_2O_2 and HSO_3^- (Loeffler & Hudson 2013). Figure 4 shows the mass-loss rate during warming of our $\text{H}_2\text{O} + \text{H}_2\text{S} + \text{O}_3$ ice mixtures from 50 to 290 K at a rate of $0.1 \text{ K minute}^{-1}$ and the O_2 (32 amu) flux measured with the MS. Over the temperature range of interest for these thermal reactions (80–130 K), there is negligible desorption from our samples, as indicated by the QCM and MS. Between 135 and 140 K, we observe our first peak in the mass-loss rate spectrum, which, based on our MS measurements, we attribute to thermally produced oxygen diffusing from our sample as the H_2O ice begins to crystallize. The desorption of trapped O_2 prior to the desorption of H_2O is consistent with previous laboratory studies examining the thermal desorption of O_2 within H_2O -ice mixtures (Vidal et al. 1997; Loeffler et al. 2006b). The presence of O_2 is also consistent with the reaction mechanisms discussed below (see Section 4.2), which yield O_2 as a major reaction product. Further warming results in two large, unresolved peaks at 155 and 160 K, which we attribute to O_2 , H_2S , and H_2O . Similar to the O_2 , residual H_2S desorbs from the ice as the H_2O crystallizes and ultimately sublimates from the sample. Following the large H_2O desorption peak, we find several additional desorption peaks that we attribute to H_2O desorbing from stable states of hydrated sulfuric acid. Based on previous studies (Moore et al. 2007; Loeffler et al. 2011), the desorption peak at 174 K is due to the decomposition of sulfuric acid tetrahydrate, while the peak at 203 K is due to the decomposition of sulfuric acid monohydrate ($\text{H}_2\text{SO}_4 \cdot 4\text{H}_2\text{O}$ and $\text{H}_2\text{SO}_4 \cdot \text{H}_2\text{O}$). We note that an additional peak occurs around 193 K. While this peak may indicate another stable hydrated state of sulfuric acid (Zhang et al. 1993), our samples were too thin at this point to allow us to determine whether there was a unique spectral signature associated with this peak (data not shown). We intend to pursue this unidentified peak further in future studies using additional chemical systems that are not oxidant-limited (e.g., $\text{H}_2\text{O}:\text{SO}_2:\text{H}_2\text{O}_2$). Once the final H_2O peak desorbs, a film of solid crystalline sulfuric acid remains until it begins to desorb at $\sim 240 \text{ K}$, which is consistent with previous studies examining the radiolytic and thermal stability of H_2SO_4 (Moore et al. 2007; Loeffler et al. 2011).

Table 1
Peak Positions for the Species Identified within $\text{H}_2\text{O} + \text{H}_2\text{S} + \text{O}_3$ Ice Mixtures at 50 K (Reactants) and 150 K (Products)

Reactants			
Species	Peak Position (cm^{-1})	Assignment	Reference
H_2O	3359	ν_1 and ν_3	Hardin & Harvey (1973); Hagen et al. (1981)
	2201	$3\nu_L$	Hardin & Harvey (1973); Ritzhaupt et al. (1976); Hagen et al. (1981)
	1654	ν_2	Hardin & Harvey (1973); Ritzhaupt et al. (1976); Hagen et al. (1981)
	806	ν_L	Bertie & Whalley (1964)
H_2S	2551	ν_1 and ν_3	Reding & Hornig (1957); Moore et al. (2007); Hudson & Gerakines (2018)
	1175	ν_2	Reding & Hornig (1957); Fathe et al. (2006); Hudson & Gerakines (2018)
O_3	1032	ν_1	Teolis et al. (2007a); Raut et al. (2011); Loeffler & Hudson (2016)
	2104	$\nu_1 + \nu_3$	Teolis et al. (2007a)
Products			
SO_2	1333	ν_3	Wiener & Nixon (1956); Moore et al. (2007)
	1149	ν_1	Wiener & Nixon (1956); Moore et al. (2007)
HSO_3^-	~ 1235	...	Moore et al. (2007); Kaňuchová et al. (2017)
	1038	...	Moore et al. (2007); Loeffler & Hudson (2016)
	1013	...	Moore et al. (2007)
HSO_4^-	~ 1235	...	Moore et al. (2007)
	1057	...	Moore et al. (2007); Loeffler & Hudson (2016)
	992	...	Loeffler & Hudson (2016)
SO_4^{2-}	1111	...	Moore et al. (2007)

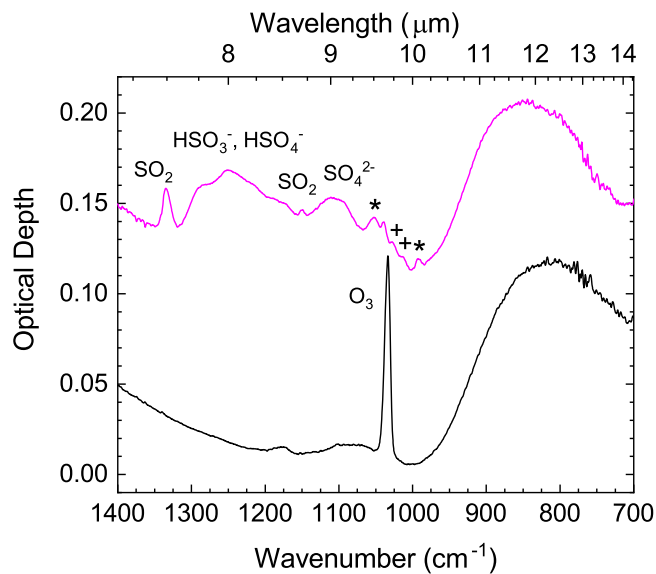


Figure 3. Mid-IR spectra of a $\text{H}_2\text{O} + \text{H}_2\text{S} + \text{O}_3$ sample (75:20:5) during warming at a rate of $0.1 \text{ K minute}^{-1}$, highlighting the spectral region containing features attributed to the sulfur products (see Table 1 for spectral assignment details). Spectra correspond to 50 (bottom) and 151 (top) K. Note that the broad and unresolved feature at 1235 cm^{-1} has been attributed to both HSO_3^- and HSO_4^- (see Table 1 for additional details). Asterisks correspond to HSO_4^- , and plus signs correspond to HSO_3^- .

4. Discussion

4.1. Reaction Chemistry and Spectral Assignments

The thermal oxidation of H_2S with O_3 has been studied in the gaseous and aqueous phases due to the reaction's implications for Earth's atmospheric chemistry (Hales et al. 1969; Glavas & Toby 1975; Mark et al. 2011); however, the exact mechanism is still unclear. Early works suggested that the primary reaction sequence produces SO_2 and O_2 through a five-membered ring (HSO_3H) and the more stable intermediates

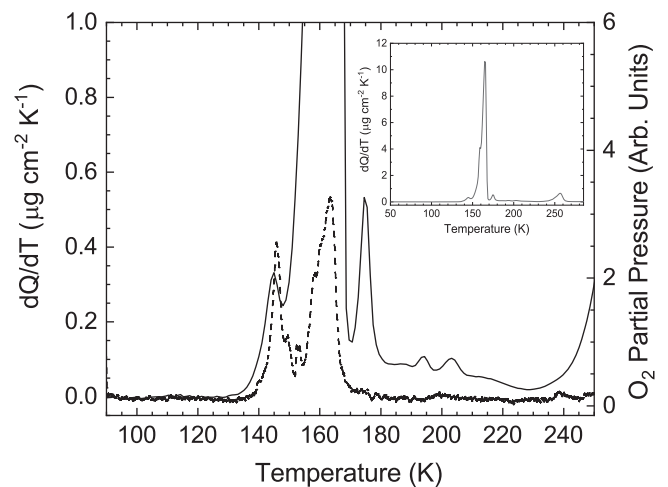
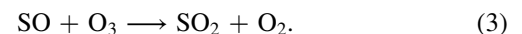


Figure 4. The QCM-derived mass-loss rate (solid line) and O_2 partial pressure (dashed line) during warming of a $\text{H}_2\text{O} + \text{H}_2\text{S} + \text{O}_3$ sample (75:20:5) at a rate of $0.1 \text{ K minute}^{-1}$. Inset: QCM-derived mass-loss rate shown in main figure but with an expanded scale to show the entire mass-loss rate curve.

HSO , HSO_2 , and SO (see Equations (1)–(3)):



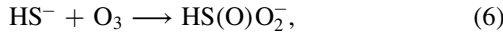
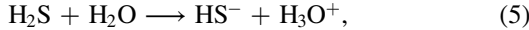
This sequence was later corroborated by chemical luminescence experiments identifying HSO within H_2S and O_3 gaseous mixtures (Schurath et al. 1977). Moreover, several previous studies have also demonstrated an oxidative addition reaction between photolyzed oxygen atoms and H_2S at low temperatures within an argon matrix forming SO_2 through the intermediate HSOH (Smardzewski & Lin 1977; Smardzewski 1978). Additionally, we note the presence of H_2O_2 in our thermally altered samples, which may form through the recombination of hydroxyl radicals formed in Equation (2)

(Loeffler et al. 2006a; Zheng et al. 2006):



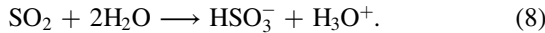
The insertion of excited oxygen radicals into water molecules is also a possible H_2O_2 formation mechanism, as suggested by Zheng et al. (2006); however, we find no evidence of the formation of H_2O_2 in our thermally altered $\text{H}_2\text{O} + \text{O}_3$ reference samples, which indicates that this formation pathway is significantly less efficient.

Mark et al. (2011) argued that the oxidation of H_2S by O_3 may primarily occur through the intermediate HS^- and a peroxysulfate anion ($\text{HS}(\text{O})\text{O}_2^-$) based on the overall molar ratio of O_3 and SO_4^{2-} within their aqueous system ($2.4 \text{ O}_3/\text{SO}_4^{2-}$ rather than the predicted $4 \text{ O}_3/\text{SO}_4^{2-}$, or a series of four O-transfer reactions):

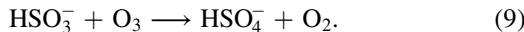


More recent computational studies agree that at low temperatures, SO_2 and H_2O are major products formed via the peroxysulfate intermediate (Mousavipour et al. 2013). We can estimate our $\text{O}_3/\text{SO}_4^{2-}$ by integrating the rate of mass-loss QCM data (Figure 4) between ~ 230 and 270 K, which is mass loss due to pure anhydrous sulfuric acid (Moore et al. 2007; Loeffler et al. 2011), and our known concentration of O_3 initially deposited at 50 K. We estimate that our $\text{O}_3/\text{SO}_4^{2-}$ molar ratio is 2.8 ± 0.6 . This molar ratio suggests that the peroxysulfate anion intermediate may also facilitate this reaction. Regardless of the mechanism, the strong SO_2 band at 1333 cm^{-1} appears in our spectra between 100 and 110 K, indicating that the H_2S is ultimately oxidized to SO_2 , producing some O_2 in the process (Moore et al. 2007).

The remainder of our reaction sequence agrees with additional atmospheric studies (Erickson et al. 1977; Hoffmann 1986) and solid-state astrochemical work (Loeffler & Hudson 2016) addressing the thermal oxidation of SO_2 , beginning with the formation of bisulfite (HSO_3^-):



Features previously attributed to bisulfite (1038 and 1235 cm^{-1} ; Moore et al. 2007; Loeffler & Hudson 2010; Kaňuchová et al. 2017; Mifsud et al. 2021b) appear in the IR spectra at nearly the exact temperature as in previous studies. Their appearance suggests that any produced SO_2 is immediately converted to HSO_3^- via autoionization of H_2O , which is consistent with work by Loeffler & Hudson (2016), where this reaction occurs at temperatures as low as 80 K. The remaining O_3 then converts the bisulfite to bisulfate (HSO_4^-), with prominent features at 992 , 1057 , and 1235 cm^{-1} . These absorption features are consistent with features found in hydrated states of sulfuric acid (Moore et al. 2007; Loeffler et al. 2011; Loeffler & Hudson 2016):



Unlike the thermal reactions within $\text{SO}_2 + \text{O}_3 + \text{H}_2\text{O}$ (Loeffler & Hudson 2016), we did not find any evidence for the sulfur anion, metabisulfite ($\text{S}_2\text{O}_5^{2-}$), within our heated ice samples, suggesting that the reaction between H_2S and O_3 does not produce enough stable bisulfite to facilitate the following

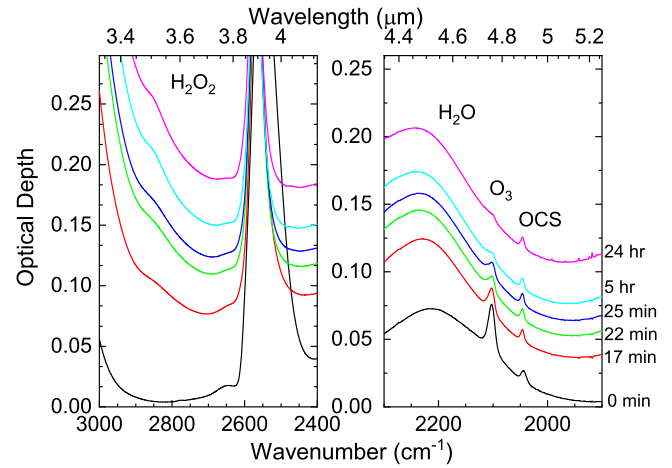
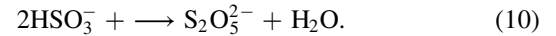


Figure 5. The IR spectra of the region containing the O_3 2104 cm^{-1} band (right) and the H_2O_2 2848 cm^{-1} band (left) in a $\text{H}_2\text{O} + \text{H}_2\text{S} + \text{O}_3$ ice during warming at 5 K minute^{-1} and isothermal annealing at 120 K . From bottom to top, these spectra correspond to the time elapsed since beginning warming: 0 minutes, 17 minutes, 22 minutes, 25 minutes, 300 minutes, and 24 hr . The first spectrum was acquired at 50 K , and the rest were acquired after equilibrating at 120 K .

reaction:



This reaction is likely limited by the number of O_3 molecules required to fully oxidize the initial H_2S .

4.2. Reaction Kinetics

Extrapolating laboratory kinetic data to astronomical temperatures and timescales is crucial for understanding thermal processes in realistic astrochemical environments. For thermal chemical reactions within the gas and aqueous phases, Arrhenius parameters (activation energy and preexponential factors) are commonly extracted from laboratory data. Though solid-state environments uniquely challenge the assumptions of Arrhenius behavior (e.g., limited motion and orientation within solids, etc.), Vyazovkin & Wight (1997) suggested that these kinetic parameters have parallels within the solid state. Some previous works have had success determining a reaction's overall activation energy by employing an isothermal annealing technique and fitting the data with first-order Arrhenius kinetics (Bossa et al. 2009; Loeffler & Hudson 2013; Noble et al. 2013). Figure 5 shows the 2104 cm^{-1} O_3 band during warming and isothermal annealing at 120 K , which we integrate after removing the linear continuum to determine the O_3 -band area, a proxy for O_3 abundance or the extent of the reaction. Figure 6 shows the normalized O_3 -band area as a function of time (50 K ; $t = 0$) for three annealing temperatures (98.5 , 105.5 , and 110.5 K). Assuming first-order Arrhenius reaction kinetics, our reaction rate constant (k) is related to our O_3 column number density by the following:

$$N(t) = N_0 e^{-kt}. \quad (11)$$

We calculate the rate constant using the time at which half of the O_3 is consumed by the reaction ($k = \frac{\ln(2)}{t_{1/2}}$). We note that for the case of 120 K , over half of the initial O_3 is consumed prior to reaching the annealing temperature. For this reason, we only use annealing temperatures below 110.5 K to calculate the reaction's activation energy.

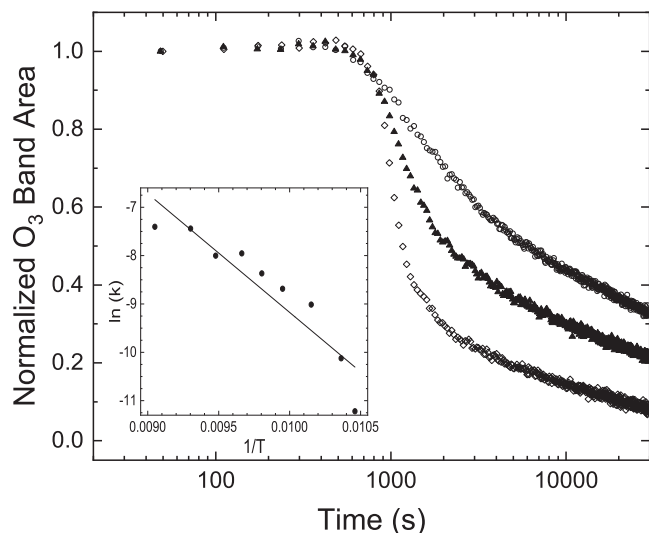


Figure 6. Normalized integrated O_3 2104 cm^{-1} band area in a $\text{H}_2\text{O} + \text{H}_2\text{S} + \text{O}_3$ ice mixture deposited at 50 K during warming at a rate of 5 K minute^{-1} to the following annealing temperatures: 98.5 K, circles; 105.5 K, triangles; 110.5 K, diamonds. Inset: Arrhenius plot of the $\text{H}_2\text{O} + \text{H}_2\text{S} + \text{O}_3$ reaction. The isothermal annealing temperatures used were 95.6, 96.5, 98.5, 100.5, 102.0, 103.5, 105.5, 107.5, and 110.5 K. The linear fit is proportional to the reaction activation energy (see text for more details). The R^2 for this linear fit is 0.86.

The inset for Figure 6 shows the Arrhenius plot for nine different annealing temperatures, where the linear fit is proportional to $-E_a/R$, and R is the universal gas constant. We derive an activation energy of $20 \pm 3\text{ kJ mol}^{-1}$, which is significantly lower than the activation energy required to oxidize SO_2 (Loeffler & Hudson 2016). Whether this difference in activation energy is due to the use of different techniques (isothermal annealing versus linear heating; Vyazovkin & Wight 1997; Loeffler & Hudson 2016) or a fundamental difference in the chemistry is something we hope to investigate in the future. Regardless, our activation energy seems reasonable compared to the literature values derived using this isothermal annealing technique (Bossas et al. 2009; Loeffler & Hudson 2013; Noble et al. 2013).

4.3. Astrophysical Implications

Our recent studies demonstrate the importance of considering low-temperature thermal reactions in astronomical environments. Specifically, H_2S is readily oxidized to sulfur anions and hydrated states of sulfuric acid in the presence of O_3 within a H_2O -ice matrix. This oxidation sequence agrees well with gas phase literature (Glavas & Toby 1975) and solid-state studies focusing on SO_2 and O_3 (Loeffler & Hudson 2016). We suspect that these results will be important not only for interpreting data from future outer solar system missions focusing on Europa, such as Europa Clipper (Phillips & Pappalardo 2014) and JUICE (Grasset et al. 2013), but also for future observations of Ganymede and Callisto, as sulfur compounds and O_3 or its precursor (O_2) are likely present and mixed within the surface of all of these satellites. Below, we discuss our results in more detail with regard to each of these three Jovian satellites.

The detection of O_2 on both hemispheres of Europa (Spencer & Calvin 2002) is expected given the strong radiation environment present on the surface (Cooper et al. 2001, 2009; Paranicas et al. 2009; Cassidy et al. 2013; Nordheim et al. 2019) and the numerous laboratory studies that have

shown that O_2 can be formed via radiolysis (H^+ , Ar^+ , and e^-) of H_2O ice (Haring et al. 1984; Sieger et al. 1998; Teolis et al. 2005; Davis et al. 2021). However, the lack of detection of O_3 on Europa is a bit more puzzling, as laboratory studies have shown that O_3 is easily produced from ion and electron irradiation of O_2 ice (Famá et al. 2002; Bennett & Kaiser 2005) and heavy ion irradiation of H_2O ice that is deposited while being actively irradiated (Teolis et al. 2006). While it is unclear why O_3 is absent on the leading hemisphere of Europa, we have noted previously that the lack of O_3 on the trailing hemisphere of Europa could be due to thermal reactions with SO_2 (Loeffler & Hudson 2016), which has been detected previously (Lane et al. 1981; Hendrix et al. 2011; Becker et al. 2022). Here we show that H_2S will also react with O_3 on the order of hours or days at the temperatures found on Europa ($\sim 90\text{--}130\text{ K}$). The potential involvement of H_2S in the thermal chemistry occurring on Europa’s surface would also explain its lack of detection on Europa, as H_2S should form from implantation of iogenic ions into the surface ice or the irradiation of other numerous sulfur-bearing compounds present (Carlson et al. 1999a, 2002; Strazzulla et al. 2009). Moreover, the radiolytic lifetime of H_2S on the surface of Europa is on the order of several years (Carlson et al. 1999a), whereas its thermal lifetime in the presence of O_3 is $\sim 5\text{ hr}$ at 120 K. These lifetimes further highlight the potentially significant role these reactions play in the overall sulfur cycle on Europa, especially below the surface, where there is significantly less radiation (Cooper et al. 2001).

For Ganymede, surface O_2 is primarily located in the middle and low latitudes of the trailing hemisphere (Trumbo et al. 2021), which is consistent with current flux models, O_2 production via the radiolysis of H_2O ice (Johnson & Jessor 1997; Poppe et al. 2018), and more recent comparisons of Ganymede’s spectra and laboratory spectra of oxygen-rich H_2O ice (Migliorini et al. 2022). Mainly, O_3 has been identified in the trailing hemisphere (Noll et al. 1996; Hendrix et al. 1999) and found to be most abundant near the poles of the trailing hemisphere (Hendrix et al. 1999). Moreover, Hendrix et al. (1999) found that the O_3 abundance correlates with the solar zenith angle, suggesting that the O_3 is destroyed by photolysis more easily at lower latitudes, where the sunlight is most intense. H_2S has also been tentatively attributed to a feature at $3.88\text{ }\mu\text{m}$ in observations of Ganymede’s surface using the Galileo NIMS instrument (McCord et al. 1998). Although the geographic distribution of this feature has not been studied, more recent work using the Very Large Telescope (Ligier et al. 2019; King et al. 2022) shows minor amounts of sulfuric acid hydrates and sulfates at low latitudes on the trailing hemisphere, which are thermal products of O_3 and H_2S , as well as reaction products between SO_2 and O_3 (Loeffler & Hudson 2016). Thus, it is also possible that the lower abundance of O_3 found at lower latitudes is due to the presence of sulfur-bearing compounds. More observational work is necessary to further constrain the compositional variation across Ganymede’s surface.

On Callisto, O_2 has been detected on the trailing side (Spencer & Calvin 2002); however, there have been no definitive detections of O_3 . Additionally, H_2S and SO_2 have been tentatively identified on Callisto using the Galileo NIMS instrument (McCord et al. 1998). While these features may be due to another species entirely (H_2CO_3 or other carbon-bearing compounds; Johnson et al. 2004) or an artifact of the method of

analysis as suggested by Hendrix & Johnson (2008), the presence of H_2S and SO_2 in the absence of O_3 is consistent with our thermal oxidation reactions.


5. Conclusions

We have shown that thermal oxidation reactions occur within $\text{H}_2\text{O} + \text{H}_2\text{S} + \text{O}_3$ ice mixtures on laboratory timescales at temperatures relevant to Europa, Ganymede, and Callisto. These reactions produce sulfur anion and O_2 products at low temperatures and hydrated sulfuric acid at higher temperatures, and the activation energy to initiate these reactions is significantly lower than the activation energy required to oxidize SO_2 to the sulfate ion. These results are generally consistent with the observed geographic distributions of sulfur compounds on the Galilean icy satellites, and this study further highlights the importance of considering thermal chemical alteration on astrophysical surfaces, despite the low temperatures. Finally, we suspect that thermal reactions with sulfur-bearing species will be important for interpreting observations made by NASA's upcoming Europa Clipper Mission, as well as future compositional investigations of the Galilean icy satellites.

This research was supported by NSF grant No. 1821919. Data from this publication can be found in Northern Arizona University's long-term repository (<https://openknowledge.nau.edu/5947>).

ORCID iDs

Patrick D. Tribbett  <https://orcid.org/0000-0001-9529-8353>

Mark J. Loeffler  <https://orcid.org/0000-0002-1551-3197>

References

- Becker, T. M., Trumbo, S. K., Molyneux, P. M., et al. 2022, *PSJ*, **3**, 129
- Behr, P. R., Tribbett, P. D., Robinson, T. D., & Loeffler, M. J. 2020, *ApJ*, **900**, 147
- Bennett, C. J., & Kaiser, R. I. 2005, *ApJ*, **635**, 1362
- Bertie, J. E., & Whalley, E. 1964, *JChPh*, **40**, 1637
- Bossa, J. B., Theulé, P., Duvernay, F., Borget, F., & Chiavassa, T. 2008, *A&A*, **492**, 719
- Bossa, J. B., Theulé, P., Duvernay, F., & Chiavassa, T. 2009, *ApJ*, **707**, 1524
- Cadle, R. D., & Ledford, M. 1966, *J. Air Water Pollut.*, **10**, 25
- Carlson, R. W., Anderson, M. S., Johnson, R. E., et al. 1999b, *Sci*, **283**, 2062
- Carlson, R. W., Anderson, M. S., Johnson, R. E., Schulman, M. B., & Yavrouian, A. H. 2002, *Icar*, **157**, 456
- Carlson, R. W., Johnson, R. E., & Anderson, M. S. 1999a, *Sci*, **286**, 97
- Caselli, P., & Ceccarelli, C. 2012, *A&ARv*, **20**, 56
- Cassidy, T. A., Paranicas, C. P., Shirley, J. H., et al. 2013, *P&SS*, **77**, 64
- Cooper, J. F., Cooper, P. D., Sittler, E. C., Sturmer, S. J., & Rymer, A. M. 2009, *P&SS*, **57**, 1607
- Cooper, J. F., Johnson, R. E., Mauk, B. H., Garrett, H. B., & Gehrels, N. 2001, *Icar*, **149**, 133
- Davis, M. R., Meier, R. M., Cooper, J. F., & Loeffler, M. J. 2021, *ApJL*, **908**, L53
- Demyk, K., Dartois, E., d'Hendecourt, L., et al. 1998, *A&A*, **339**, 553
- Earle, A. M., Binzel, R. P., Young, L. A., et al. 2017, *Icar*, **287**, 37
- Erickson, R. E., Yates, L. M., Clark, R. L., & McEwen, D. 1977, *AtmEn*, **11**, 813
- Famá, M., Bahr, D. A., Teolis, B. D., & Baragiola, R. A. 2002, *NIMPA*, **193**, 775
- Fathe, K., Holt, J. S., Oxley, S. P., & Pursell, C. J. 2006, *JPCA*, **110**, 10793
- Ferrante, R. F., Moore, M. H., Spiliotis, M. M., & Hudson, R. L. 2008, *ApJ*, **684**, 1210
- Gerakines, P. A., & Hudson, R. L. 2015, *ApJL*, **808**, L40
- Gerakines, P. A., Schutte, W. A., Greenberg, J. M., & van Dishoeck, E. F. 1995, *A&A*, **296**, 810
- Ghosh, D., Mondal, B., Bagchi, S., & Kumar Das, A. 2010, *MolPh*, **108**, 3353
- Glavas, S., & Toby, S. 1975, *JPhCh*, **79**, 779
- Grasset, O., Dougherty, M., Coustenis, A., et al. 2013, *P&SS*, **78**, 1
- Greeley, R., Chyba, C. F., Head, J., et al. 2004, in *Jupiter: The Planet, Satellites and Magnetosphere*, ed. F. Bagenal, T. E. Dowling, & W. B. McKinnon (Cambridge: Cambridge Univ. Press), 329
- Hagen, W., Tielens, A. G. G. M., & Greenberg, J. M. 1981, *CP*, **56**, 367
- Hales, J. M., Wilkes, J. O., & York, J. L. 1969, *AtmEn*, **3**, 657
- Hand, K. P., & Brown, M. E. 2013, *ApJL*, **766**, L21
- Hanel, R., Conrath, B., Flasar, F., et al. 1982, *Sci*, **215**, 544
- Hardin, A. H., & Harvey, K. B. 1973, *AcSpA*, **29**, 1139
- Haring, R. A., Kofschoten, A. W., & De Vries, A. E. 1984, *NIMPB*, **2**, 544
- Hendrix, A. R., Barth, C. A., & Hord, C. W. 1999, *JGR*, **104**, 14169
- Hendrix, A. R., Cassidy, T. A., Johnson, R. E., Paranicas, C., & Carlson, R. W. 2011, *Icar*, **212**, 736
- Hendrix, A. R., & Johnson, R. E. 2008, *ApJ*, **687**, 706
- Hoffmann, M. R. 1986, *AtmEn*, **20**, 1145
- Hudson, R. L., & Gerakines, P. A. 2018, *ApJ*, **867**, 138
- Jiménez-Escobar, A., & Muñoz Caro, G. M. 2011, *A&A*, **536**, A91
- Johnson, R. E., Carlson, R. W., Cooper, J. F., et al. 2004, in *Jupiter: The Planet, Satellites and Magnetosphere*, ed. F. Bagenal, T. E. Dowling, & W. B. McKinnon (Cambridge: Cambridge Univ. Press), 485
- Johnson, R. E., & Jessor, W. A. 1997, *ApJ*, **480**, L79
- Kaňuchová, Z., Boduch, P., Domaracka, A., et al. 2017, *A&A*, **604**, A68
- King, O., Fletcher, L. N., & Ligier, N. 2022, *PSJ*, **3**, 72
- Lane, A. L., Nelson, R. M., & Matson, D. L. 1981, *Natur*, **292**, 38
- Ligier, N., Paranicas, C., Carter, J., et al. 2019, *Icar*, **333**, 496
- Loeffler, M. J., Hudson, R. L., Moore, M. H., & Carlson, R. W. 2011, *Icar*, **215**, 370
- Loeffler, M. J., Moore, M. H., & Gerakines, P. A. 2016, *ApJ*, **827**, 98
- Loeffler, M. J., Raut, U., Vidal, R. A., Baragiola, R. A., & Carlson, R. W. 2006a, *Icar*, **180**, 265
- Loeffler, M. J., Teolis, B. D., & Baragiola, R. A. 2006b, *ApJL*, **639**, L103
- Loeffler, M. J., & Hudson, R. L. 2010, *GeoRL*, **37**, L19201
- Loeffler, M. J., & Hudson, R. L. 2013, *Icar*, **224**, 257
- Loeffler, M. J., & Hudson, R. L. 2015, *AsBio*, **15**, 453
- Loeffler, M. J., & Hudson, R. L. 2016, *ApJL*, **833**, L9
- Mahjoub, A., & Hodyss, R. 2018, *ApJ*, **869**, 98
- Mark, G., Naumov, S., & von Sonntag, C. 2011, *Ozone: Science & Engineering*, **33**, 37
- McCord, T. B., Hansen, G. B., Clark, R. N., et al. 1998, *JGR*, **103**, 8603
- Mifsud, D. V., Juhász, Z., Herczku, P., et al. 2021b, *EPJD*, **75**, 182
- Mifsud, D. V., Kaňuchová, Z., Herczku, P., et al. 2021a, *SSRv*, **217**, 1
- Migliorini, A., Kanuchova, Z., Ioppolo, S., et al. 2022, *Icar*, **383**, 115074
- Moore, M. H., & Hudson, R. L. 2000, *Icar*, **145**, 282
- Moore, M. H., Hudson, R. L., & Carlson, R. W. 2007, *Icar*, **189**, 409
- Mousavipour, S. H., Mortazavi, M., & Hematti, O. 2013, *JPCA*, **117**, 6744
- Noble, J. A., Theule, P., Mispelaer, F., et al. 2012, *A&A*, **543**, A5
- Noble, J. A., Theule, P., Borget, F., et al. 2013, *MNRAS*, **428**, 3262
- Noll, K. S., Roush, T. L., Cruikshank, D. P., Johnson, R. E., & Pendleton, Y. J. 1997, *Natur*, **388**, 45
- Noll, K. S., Johnson, R. E., Lane, A. L., Domingue, D. L., & Weaver, H. A. 1996, *Sci*, **273**, 341
- Nordheim, T. A., Jasinski, J. M., & Hand, K. P. 2019, *ApJL*, **881**, L29
- Orlando, T. M., & Sieger, M. T. 2003, *SurSc*, **528**, 1
- Paranicas, C., Cooper, J., Garrett, H., Johnson, R., & Sturmer, S. 2009, in *Europa*, ed. R. T. Pappalardo et al. (Tucson, AZ: Univ. Arizona Press), 529
- Phillips, C. B., & Pappalardo, R. T. 2014, *EOSTr*, **95**, 165
- Poppe, A. R., Fatemi, S., & Khurana, K. K. 2018, *JGRA*, **123**, 4614
- Raut, U., Loeffler, M. J., Famá, M., & Baragiola, R. A. 2011, *JChPh*, **134**, 194501
- Reding, F. P., & Hornig, D. F. 1957, *JChPh*, **27**, 1024
- Ritzhaupt, G., Smyrl, N., & Devlin, J. P. 1976, *JChPh*, **64**, 435
- Schurath, U., Weber, M., & Becker, K. H. 1977, *JChPh*, **67**, 110
- Sieger, M. T., Simpson, W. C., & Orlando, T. M. 1998, *Natur*, **394**, 554
- Smardzewski, R. R., & Lin, M. C. 1977, *JChPh*, **66**, 3197
- Smardzewski, R. R. 1978, *JChPh*, **68**, 2878
- Spencer, J. R., & Calvin, W. M. 2002, *AJ*, **124**, 3400
- Spencer, J. R., Tamppari, L. K., Martin, T. Z., & Travis, L. D. 1999, *Sci*, **284**, 5419
- Squyres, S. W. 1980, *Icar*, **44**, 502
- Stern, S. A., Weintraub, D. A., & Festou, M. C. 1993, *Sci*, **261**, 1713
- Strazzulla, G., Garozzo, M., & Gomis, O. 2009, *AdSpR*, **43**, 1442
- Teolis, B. D., Famá, M., & Baragiola, R. A. 2007a, *JChPh*, **127**, 074507
- Teolis, B. D., Loeffler, M. J., Raut, U., Famá, M., & Baragiola, R. A. 2007b, *Icar*, **190**, 274

- Teolis, B. D., Vidal, R. A., Shi, J., & Baragiola, R. A. 2005, [PhRvB](#), **72**, [245422](#)
- Teolis, B. D., Loeffler, M. J., Raut, U., Fama, M., & Baragiola, R. A. 2006, [ApJL](#), **644**, [L141](#)
- Theulé, P., Duvernay, F., Danger, G., et al. 2013, [AdSpR](#), **52**, [1567](#)
- Tribbett, P. D., & Loeffler, M. J. 2021, [SurSc](#), **707**, [121797](#)
- Tribbett, P. D., Tegler, S. C., & Loeffler, M. J. 2021, [ApJ](#), **915**, [40](#)
- Trumbo, S. K., Brown, M. E., & Adams, D. 2021, [PSJ](#), **2**, [139](#)
- Vidal, R. A., Bahr, D., Baragiola, R. A., & Peters, M. 1997, [Sci](#), **276**, [1839](#)
- Vyazovkin, S., & Wight, C. A. 1997, [ARPC](#), **48**, [125](#)
- Westley, M. S., Baratta, G. A., & Baragiola, R. A. 1998, [JChPh](#), **108**, [3321](#)
- Wiener, R. N., & Nixon, E. R. 1956, [JChPh](#), **25**, [175](#)
- Yarnall, Y. Y., & Hudson, R. L. 2022a, [Icar](#), **373**, [114799](#)
- Yarnall, Y. Y., & Hudson, R. L. 2022b, [ApJL](#), **931**, [L4](#)
- Zhang, R., Wooldridge, P. J., Abbatt, J. P., & Molina, M. J. 1993, [JPhCh](#), **97**, [7351](#)
- Zheng, W., Jewitt, D., & Kaiser, R. I. 2006, [ApJ](#), **639**, [534](#)
- Zheng, W., & Kaiser, R. I. 2007, [CPL](#), **450**, [55](#)